

21179
L.3

ROCK MATRIX AND FRACTURE ANALYSIS OF FLOW IN
WESTERN TIGHT GAS SANDS

DOE/MC/21179--T6

DE92 017656

Quarterly Technical Progress Report
September & December 1984

N. R. Morrow
K. R. Brower
N. H. Kilmer
J. S. Ward

New Mexico Petroleum Recovery Research Center
New Mexico Institute of Mining and Technology
Socorro, New Mexico

Contributors:

Shirleen Bretz
Vijaya Dandge
Mary Graham
Deborah Hagen

7/28/92

QEB

PRRC Report 83-14

Prepared for the Department of Energy
Under Contract No. DE-AC21-84MC21179

MASTER

NOTICE

This report was prepared as an account of work sponsored by an agency of the United States Government. Neither the United States Government nor any agency thereof, nor any of their employees, makes any warranty, express or implied, or assumes any legal liability or responsibility for the accuracy, completeness, or usefulness of any information, apparatus, product, or process disclosed, or represents that its use would not infringe privately owned rights. Reference herein to any specific commercial product, process, or service by trade name, trademark, manufacturer, or otherwise, does not necessarily constitute or imply its endorsement, recommendation, or favoring by the United States Government or any agency thereof. The views and opinions of authors expressed herein do not necessarily state or reflect those of the United States Government or any agency thereof.

DISTRIBUTION OF THIS DOCUMENT IS UNLIMITED

ok

Initial work on this project has been focussed on Tasks 2 and 4 because of strong interest in the effects of natural fractures and water on gas production.

Task 2. Flow Along and Across Fractures

Sometimes production from low permeability gas sands is much higher than could be expected from the properties of the rock matrix as determined by core analysis. The presence of natural fractures is often cited as a key factor in gas production for both fractured and unfractured wells. Numerous vertical fractures have been found in cores recovered in the Multi-Well Project. The cores show that by far the majority of fractures become filled with calcite cement. However, calcite-filled fractures are not necessarily a seal to gas flow.

As part of this project, flow measurements are being made along and across selected fractured samples as a function of overburden pressure for a minimum of five core samples. Comparative measurements will be made on unfractured neighboring cores. Permeability measurements will be made at a minimum of four levels of water saturation for each of at least six samples to assess the effect of water content on permeabilities in fractured systems. The effects of chemical treatments on mineralized fractures will be studied to assess whether such treatments lead to permeability enhancement or formation damage.

Progress

Two samples from MWX 1 13-18 have been tested thus far to compare flow in fractured samples to neighboring samples without fractures. In this case the sample cores were taken vertically, so that the mineralized fracture runs along the length of the sample. Figure 1 shows permeabilities measured for the unfractured sample with confining pressures up to 5000 psi and water saturations up to 60%. Figure 2 shows data for the same conditions in the corresponding fractured sample.

There appears to be a difference in the change in pressure sensitivity with increasing water saturation for these two samples. The unfractured sample has slightly less response to changes in confining pressure and lower initial permeability than the fractured core. This is

indicated by the steeper slope of the log-log plot in Figure 2 than in Figure 1 for the 0% water saturation cases. As water is added to the samples, however, the pressure sensitivity becomes greater in the unfractured sample. It may also be noted that a linear relationship pertains in these log-log plots of permeability versus confining pressure with convergence of the lines very roughly at around 100 psi. Table 1 shows the results of least squares fits to all these lines and the projected permeabilities at 100 psi. It is not possible to predict, from this initial case, whether these observations will prove to be true in general for fractured and unfractured samples. Further tests are required to confirm the results reported here.

Task 4. Effect of Water on Gas Production

Water is known to modify greatly the flow of gas in tight sand and is a key factor in gas production. Permeability to gas will be measured at various levels of water saturation established by equilibration of core samples in humidity chambers. Electrical resistivity at various levels of water saturations and confining pressures will also be measured. Special attention will be given to water distribution within the rock pore space. Circumstances under which water can act to inhibit gas production and the pressure differences necessary to overcome capillary seals formed by water will also be investigated. Capillary pressure measurements will be made using a high-speed centrifuge.

Progress

Permeability Measurements: Permeabilities to nitrogen at confining pressures of 500 and 5000 psi have been measured for four Multi-Well core samples. Single phase gas permeabilities measured in dry cores showed the hysteresis between first and subsequent cycles of confining pressure loading as reported previously.¹ Repetition of first loading results probably requires that the core samples stand for weeks at ambient conditions. Thus the results of second and subsequent loading cycles are more readily obtained and repeated and are therefore used for comparative purposes. Loading history is included with permeability measurements (as given for example, in Table 2). K_{∞} denotes permeabilities extrapolated to infinite pressure; other K values are measured at a single, fairly high pressure (usually about 350 psi) and are therefore close to K_{∞} values.

Partial water saturations were established in these same four core samples in order to determine gas permeabilities in the presence of varying amounts of water. Nominal saturations of 60, 45, 30 and 15% were reached by evaporation from an initially water saturated core. The time required to reach a specified saturation depended on the core permeability and the initial and final saturations.

In all cases, measurement on oven dried samples was made first, followed by saturation of the sample and partial evaporation first to 60% water saturation. Successively lower water saturations (45, 30 and 15%) were tested in that order. Successive loading cycles are reported at each step, but only for the dry core is there really a first loading measurement in the sense that the core has been at ambient conditions for a long period before testing. Results are reported in Table 2.

With only a few exceptions, the results show the expected trends. Permeability decreases as water saturation increases above 15%. Second loading permeabilities at 15% saturation are similar to or slightly higher than in the dry cores indicating that this amount of water has very little effect on gas flow. At 30% water saturation, a definite depression of the permeability is evident. This trend continues until at 60% water saturation little or no nitrogen flows, especially at high confining pressure.

Of the four samples tested, only three have significant permeabilities to gas before addition of water. Sample MWX 3 66-17, which has a porosity of only 3.02%, had less than a tenth of a microdarcy permeability to nitrogen when the core was dry. Water saturation has little further effect in reducing this permeability until fairly high saturation is reached.

The other three samples exhibit consistent changes in relative permeability and pressure sensitivity with changes in water saturation. Figures 3-5 show relative permeability plotted as a function of water saturation for MWX 3 64-29, MWX 3 67-16 and MWX 3 67-35 at both 500 and 5000 psi confining pressure.

One trend in these results for the few samples studied to date is an apparent relationship between the porosity of these samples and the way relative permeability changes with water saturation and confining pressure. MWX 3 64-29, the sample with lowest porosity of the three, shows the greatest difference in permeabilities between confining pressures of 500 and 5000 psi. Relative permeability decreases much more steeply with increasing water saturation at high confining pressure than it does at 500 psi (Figure 3). MWX 3 67-35, the sample with highest porosity, shows changes in relative permeability which depend primarily on water saturation and only slightly on confining pressure (Figure 4). MWX 3 67-16, intermediate in porosity, also shows behavior intermediate in pressure dependence (Figure 5).

Pressure sensitivity is more directly shown in Figure 6 where the ratio of permeability at 500 psi to that at 5000 psi for second or subsequent loadings is plotted as a function of water saturation for all three samples. Again, MWX 3 67-35 is least pressure sensitive and MWX 64-29 is most influenced by confining pressure at all water saturations. The pressure sensitivity index provided by this ratio is nearly linear for all three samples to a water saturation of 45%, and beyond for the two less sensitive samples.

Capillary Pressures: Prior to inception of the work on the current contract, studies were made using a high-speed centrifuge to determine capillary pressure as a function of water saturation for a suite of Multi-Well cores. Results of those studies are included here along with current results to provide as complete a picture as possible of the

capillary pressure relationships in these samples. Figures 7-13 summarize the data obtained through this quarter. Included are results of centrifuge studies with an aqueous phase (8% KNO_3) displaced by air, decane displaced by air and desorption studies in constant humidity environments. Three samples from the coastal zone, three paludal samples and one higher permeability paralic zone sample, are included in this study. Table 3 lists properties of these cores; fluid properties are given in Table 4. Details of the centrifuge procedure and data reduction process have been discussed previously¹ and are in accordance with Beckman's recommendations² and the Hassler-Brunner method³ of data handling.

These summary plots show that scatter in the data is regularly observed, and put boundaries on the amount of uncertainty associated with the measurement and data reduction process as applied to tight sandstones. Data at the highest rotational speeds are not interpretable by the standard Hassler-Brunner method and are not included in these plots.

One question which arose in measurements using the high-speed centrifuge for low permeability sandstones is the length of time required to establish a new saturation distribution as rotational speed is increased. Approach to the final saturation is likely to be slower for these samples than for the more permeable sandstones discussed in the literature. Figures 14a and 14b illustrate two cases where data were taken over 8 to 24 hour spans to allow observation of trends of fluid expelled as a function of inverse time at a given rotational speed. The data reported here are for successive measurements of MWX 2 51-19 with air

displacing decane. A reasonably linear trend is observed for times greater than one hour and in most cases a projection can be made from the measurements for up to 8 hours which agrees well with the value measured after 24 hours. As shown in Figure 14b, approach to a final reading often takes place more rapidly at higher rotational speeds.

Figures 7-13 include data for air displacing decane in addition to that for air displacing brine. These two cases may be compared more directly on the basis of displacement curvature which in identical samples would be proportional to the ratio of capillary pressure and surface tension. Figure 15 is an example of the results of comparisons between displacement curvatures for brine and decane. Ideally, these should be the same for identical porous media. In fact, different core samples, cut from the same whole core were used as shown. Nevertheless, the decane results are always significantly below those for brine at the same saturation. Tests with other fluids in these same cores are underway to determine whether fluid polarity influences measurements in these tight gas sands.

REFERENCES

Ward, J. S. and Morrow, N. R., "Multiwell Special Core Analysis," PRRC Report #84-25, October 1, 1984.

Skuse, B., "Capillary Pressure Measurements in Reservoir Rock Cores Using the Centrifuge," Beckman Applications Data, DS-607, not dated.

Hassler, G. L. and Brunner, E., "Measurement of Capillary Pressure in Small Core Samples," Trans. AIME, Vol 160, 114-123 (1945).

Table 1

Least-Squares Fits to Permeability vs. Confining Pressure Data
for MWX 1 13-18 Vertical Samples With (V*) and Without (V) Fractures

		(in the form $K = a P^b$)			k_{100}
		<u>a</u>	<u>b</u>	<u>r²</u>	<u>(extrapolated)</u>
V*		773	- .835	.993	16.5
		1483	- .985	.998	15.9
		3815	-1.17	.996	17.8
		10109	-1.36	.995	19.4
		12165	-1.42	.990	17.5
V		136	- .642	.998	7.11
		468	- .894	.997	7.65
		1095	-1.09	.976	7.12
		7609	-1.49	.988	7.88
		6410	-1.65	1.0	3.15

Table 2

Permeabilities as a Function of Confining Pressure and Water Saturation

Sample	S_w		K_{500} (μd)	K_{5000} (μd)	Loading Cycles at this S_w	Total Loading Cycles	$\frac{K_{500}}{K_{5000}}$ (and Loading)
	Initial	Final					
MWX-3 66-17 $\phi = 3.02\%$	0	0	1.68*	0.025*	1	1	3.45
			0.076*	0.022*	2	2	
	60	57.96	0.675*	0.0133	1	3	1.92
			0.0275*	0.0143	2	4	
	45	41.58	0.445*	0.016*	1	5	3.43
			0.060*	0.0175*	2	6	
	33	34.68	0.090*	0.0195*	1	7	3.18
			0.070*	0.022*	2	8	
	15	17.02	0.12*	0.028*	1	9	5.10
			0.102*	0.020	2	10	
MWX-3 64-29 $\phi = 8.64\%$	0	0	31.6	2.29	1	1	4.25
			11.6	2.66	2	2	
	60	58.27	4.83	-	1	3	44.0
			5.659	-	2	4	
	45	44.25	6.00	0.107	1	5	44.0
			5.10	0.116	2	6	
	30	28.91	11.6	0.895	1	7	12.4
			11.0	0.889	2	8	
	15	14.64	16.5	1.71	1	9	8.49
			14.6	1.72	2	10	

* K_∞

Table 2 (continued)

Sample	S_w		K_{500} (μd)	K_{5000} (μd)	Loading Cycles at this S_w	Total Loading Cycles	$\frac{K_{500}}{K_{5000}}$ (and loading)
	Initial	Final					
MWX-3 67-16 $\phi = 10.35\%$	0	0	22.0	4.70	1	1	2.37
			10.1	4.27	2	2	
	60	58.83	2.15	-	1	3	
			0.132	-	2	4	
	45	43.21	2.84	0.413	1	5	5.08
			2.09	0.411	2	6	
	30	28.52	6.72	1.48	1	7	4.08
			6.32	1.55	2	8	
	15	14.66	10.6	3.18	1	9	3.07
			9.79	3.19	2	10	
MWX-3 67-35 $\phi = 11.83\%$	0	0	27.0*	11.0*	1	1	1.58
			17.4*	11.0*	2	2	
	60	44.88	2.40*	0.440*	1	3	2.38
			1.90*	0.800*	2	4	
	30	26.46	13.6*	7.5*	1	5	1.73
			13.0*	7.5*	2	6	
	15	14.27	20.6*	11.2*	1	7	2.78
			20.6*	11.0*	2	8	

* K_{∞}

Table 3

CORE PROPERTIES

ID			Porosity (%)	BET Surface Area (m ² /g)		Length (cm)	Pore Volume (ml)
MWX-1	42-25	Coastal	7.92	2.65	A	2.26	.844 ± .007
					B	1.95	.708 ± .002
MWX-2	51-19	Coastal	7.52	2.20	C	2.63	1.071 ± .003
					D	2.85	1.165 ± .009
MWX-3	64-29	Coastal	8.64	4.35	E	2.70	1.136 ± .009
					F	2.70	1.140 ± .008
MWX-3	66-17	Paludal	3.02	2.59	BB	2.54	.290
					CC	2.54	.290
					DD	2.38	.330
MWX-3	67-16	Paludal	10.35	3.50	AA	2.46	1.253 ± .014
					GG	2.50	1.313 ± .005
MWX-3	67-35	Paludal	11.83	3.02	EE	2.53	1.481 ± .038
					FF	2.43	1.490 ± .010
MWX-1	3-25	Pualic	9.43	1.30	H	2.42	1.10
					I	2.41	1.07
					J	2.43	1.11

Table 4

FLUID PROPERTIES

	Surface Tension (dynes/cm)	Density at 25°C
8% KNO ₃ + 200 ppm NaN ₃	71.2	1.044
n-decane	23.7	.730

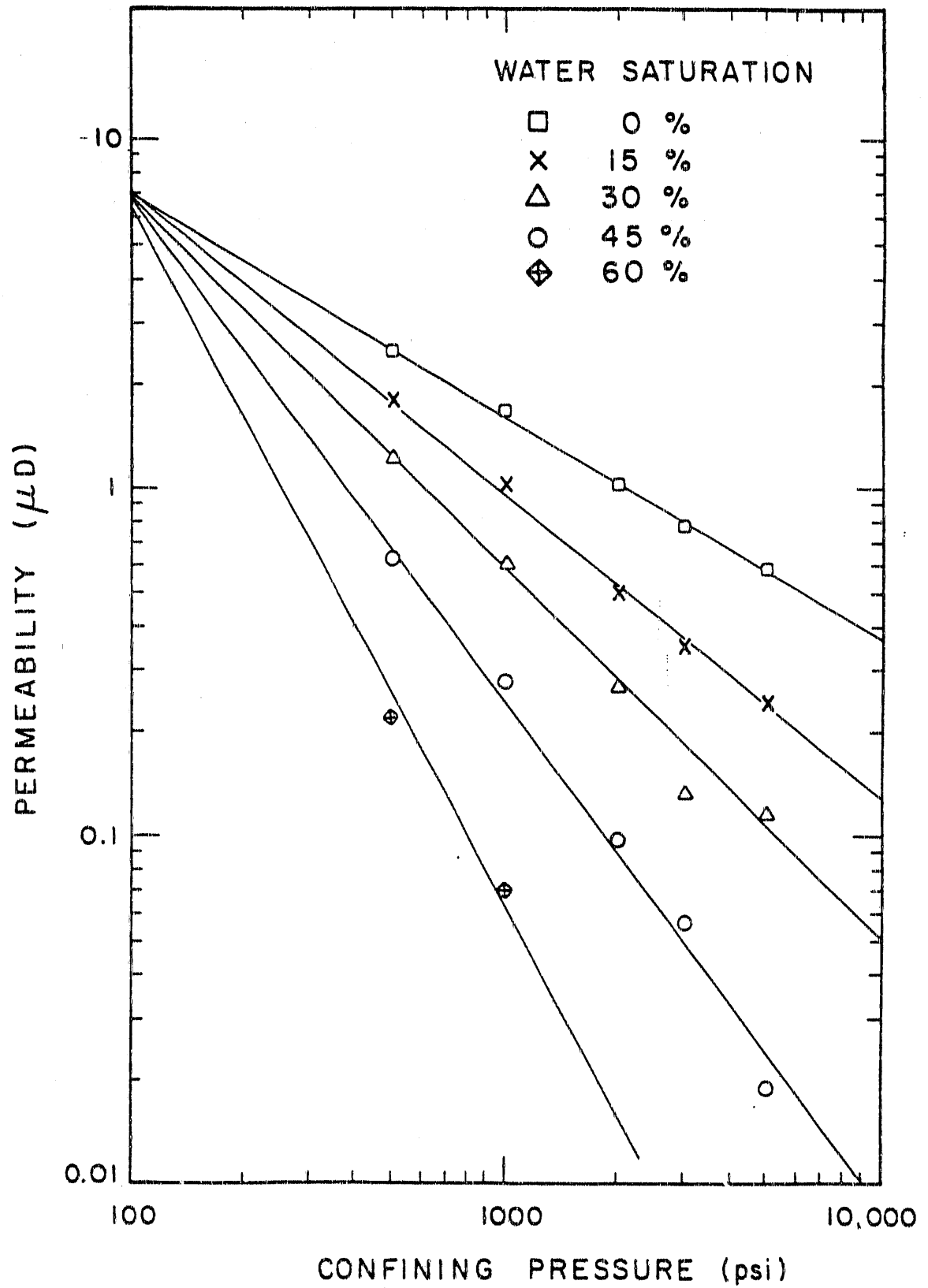


Figure 1 Gas permeability as a function of confining pressure with established water saturations from 0 to 60% for MWX 1 13-18 v, a vertical core plug with no fracture.

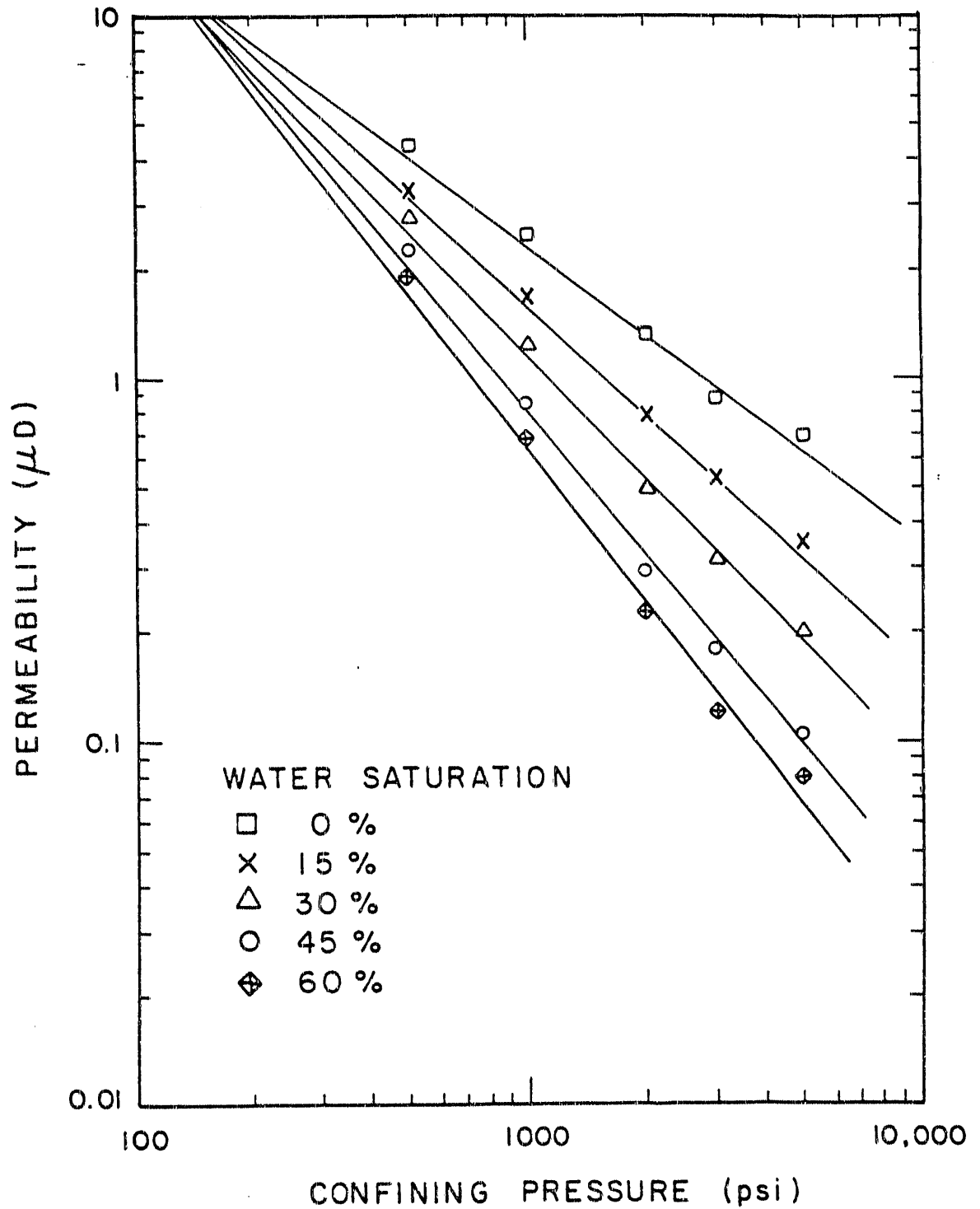


Figure 2 Gas permeability as a function of confining pressure with established water saturations from 0 to 60% for MWX 1 13-18 V*, a vertical core plug with a calcite-filled fracture.

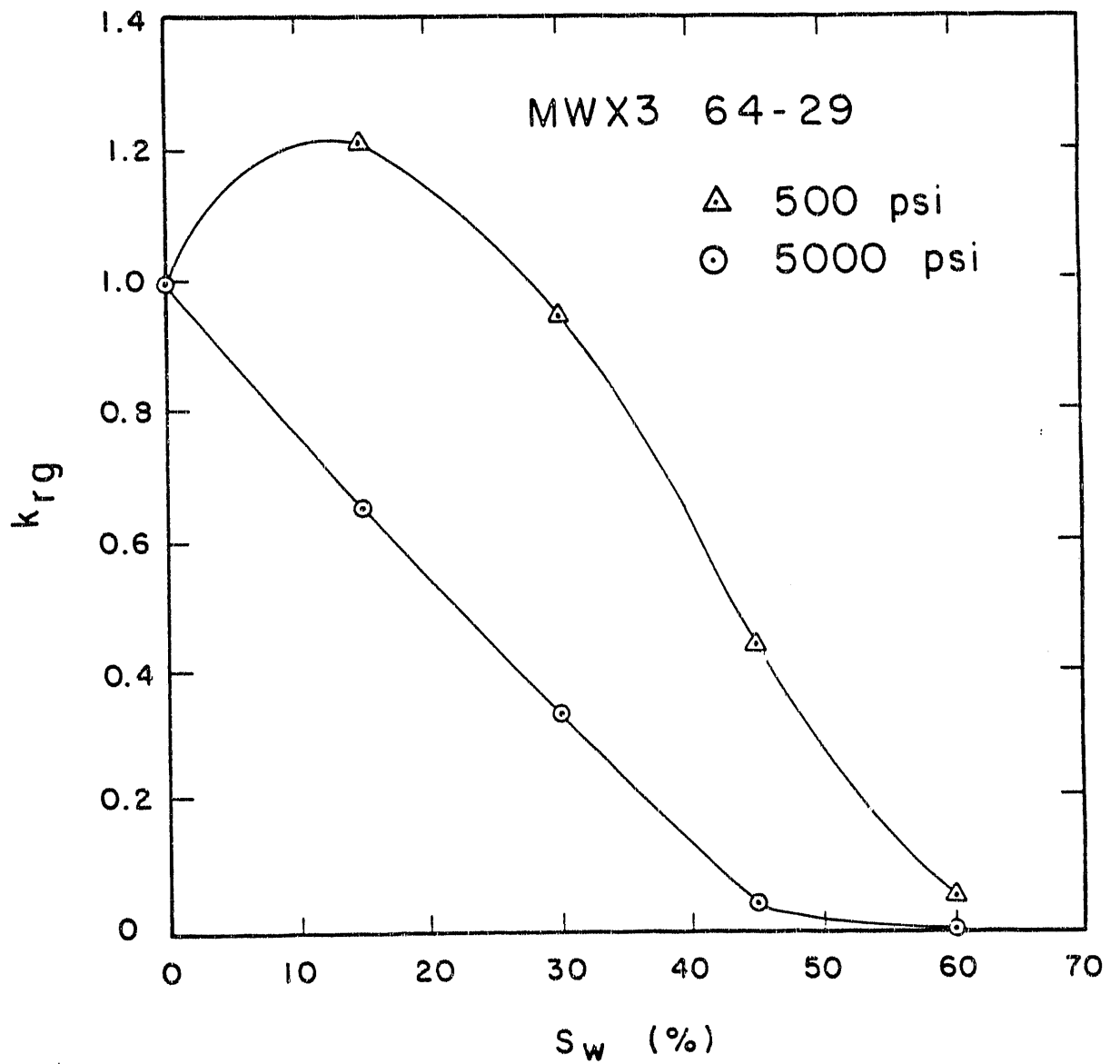


Figure 3 Relative permeability to nitrogen as a function of established water saturation at confining pressures of 500 and 5000 psia for MWX 3 64-29.

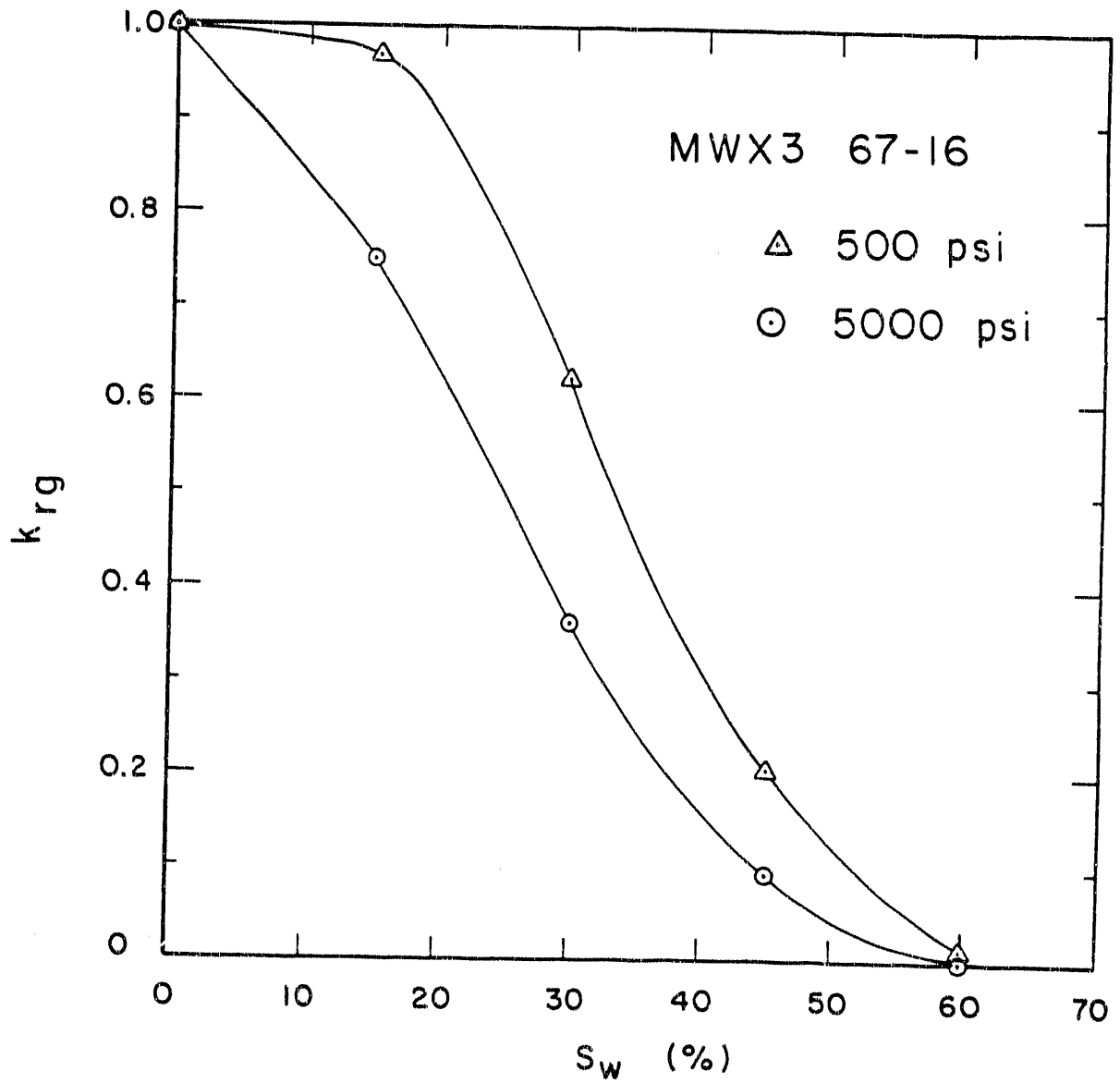


Figure 4 Relative permeability to nitrogen as a function of established water saturation at confining pressures of 500 and 5000 psia for MWX 3 67-16.

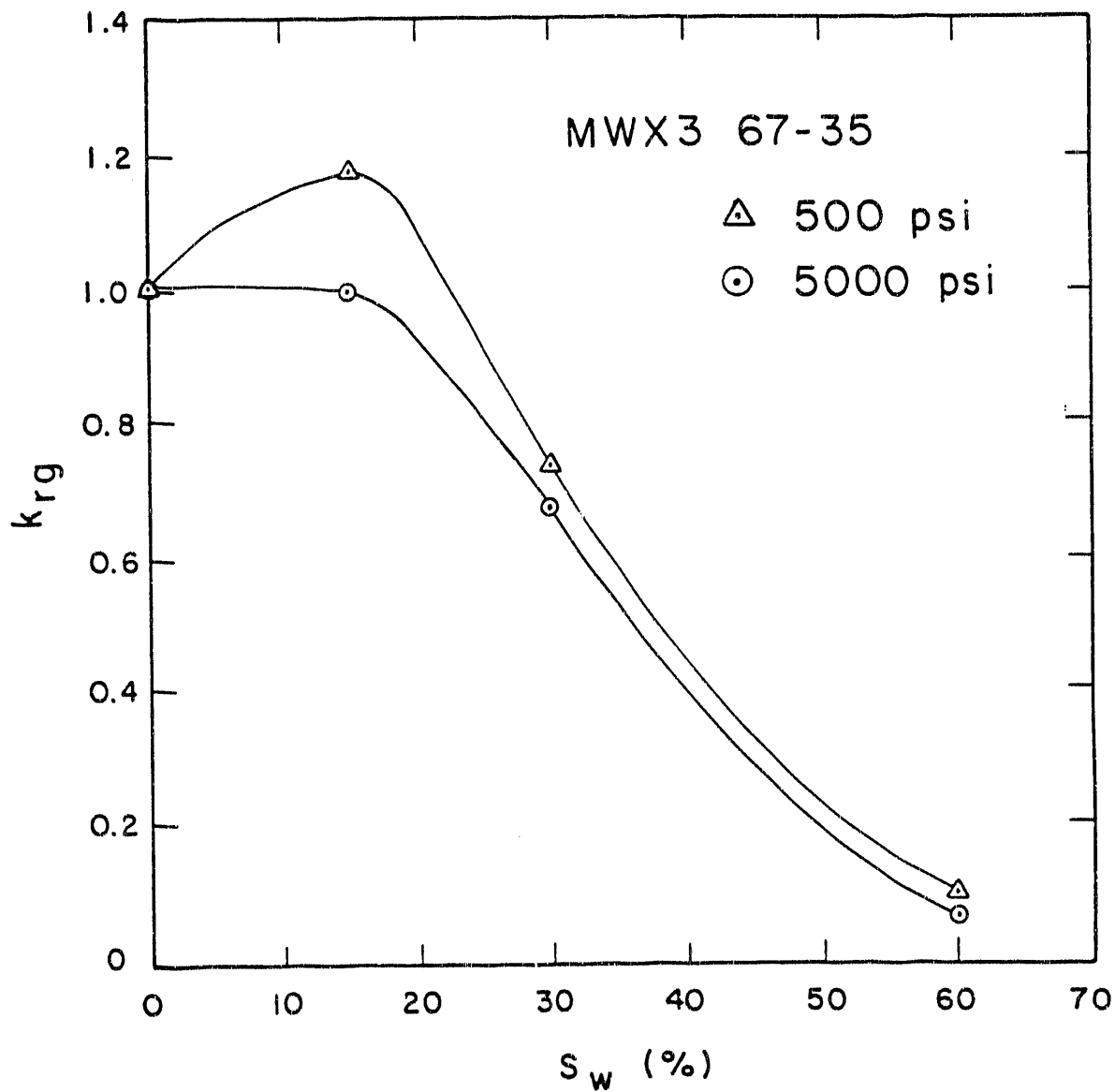


Figure 5 Relative permeability to nitrogen as a function of established water saturation at confining pressures of 500 and 5000 psia for MWX 3 67-35.

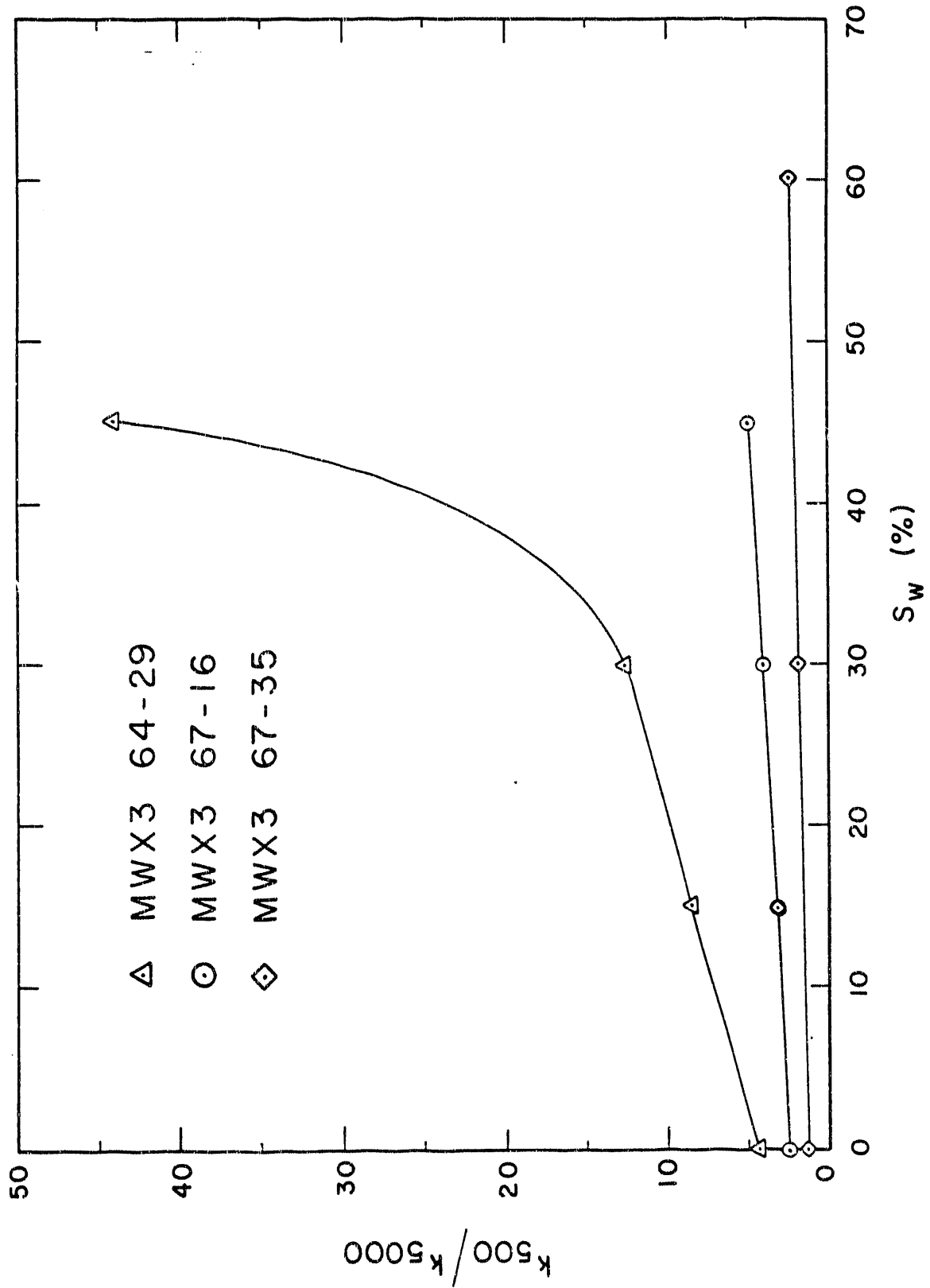


Figure 6 Pressure sensitivity for three multiwell samples with established water saturations.

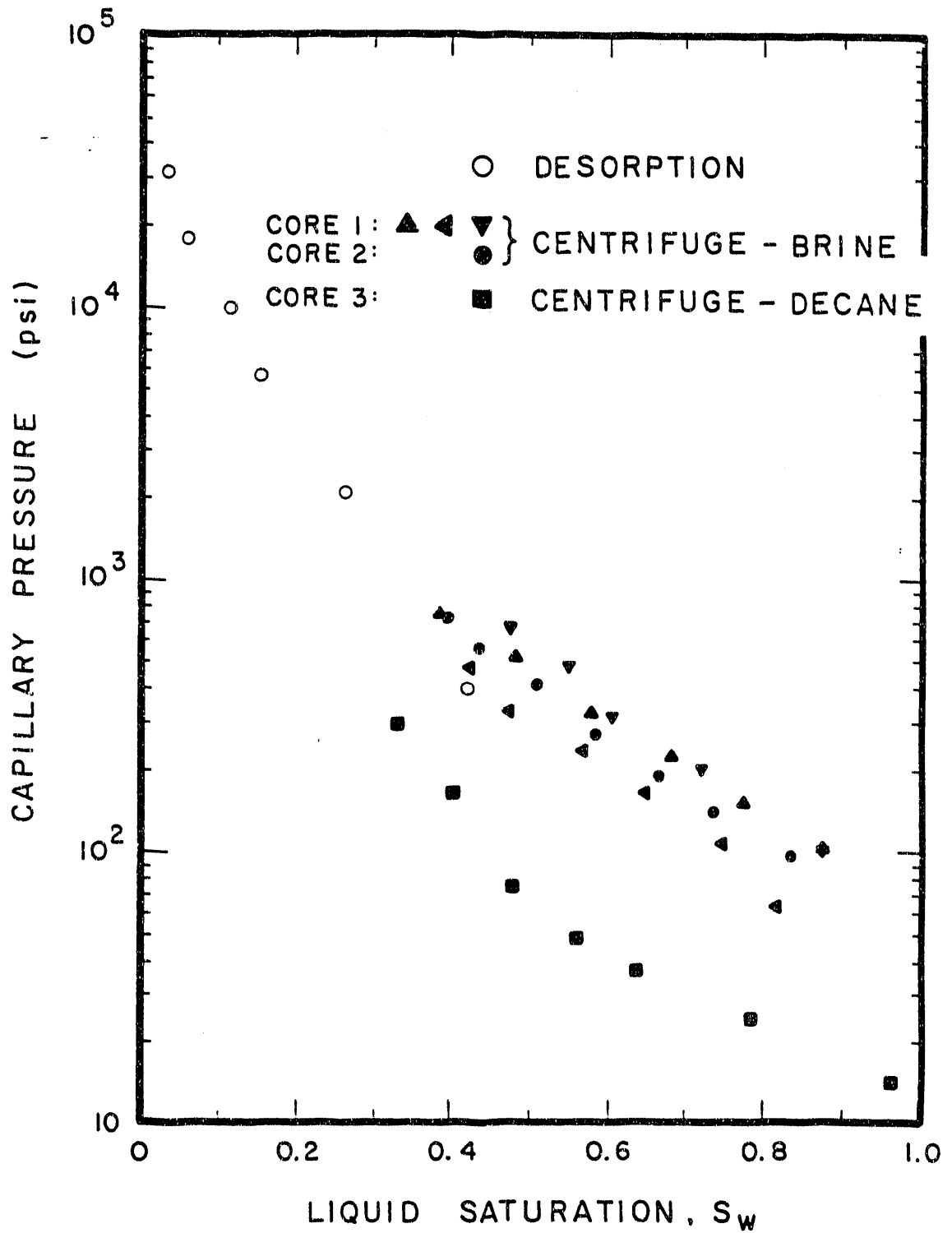


Figure 7

Capillary pressure by combination of centrifuging and desorption: MWXI 42-25.

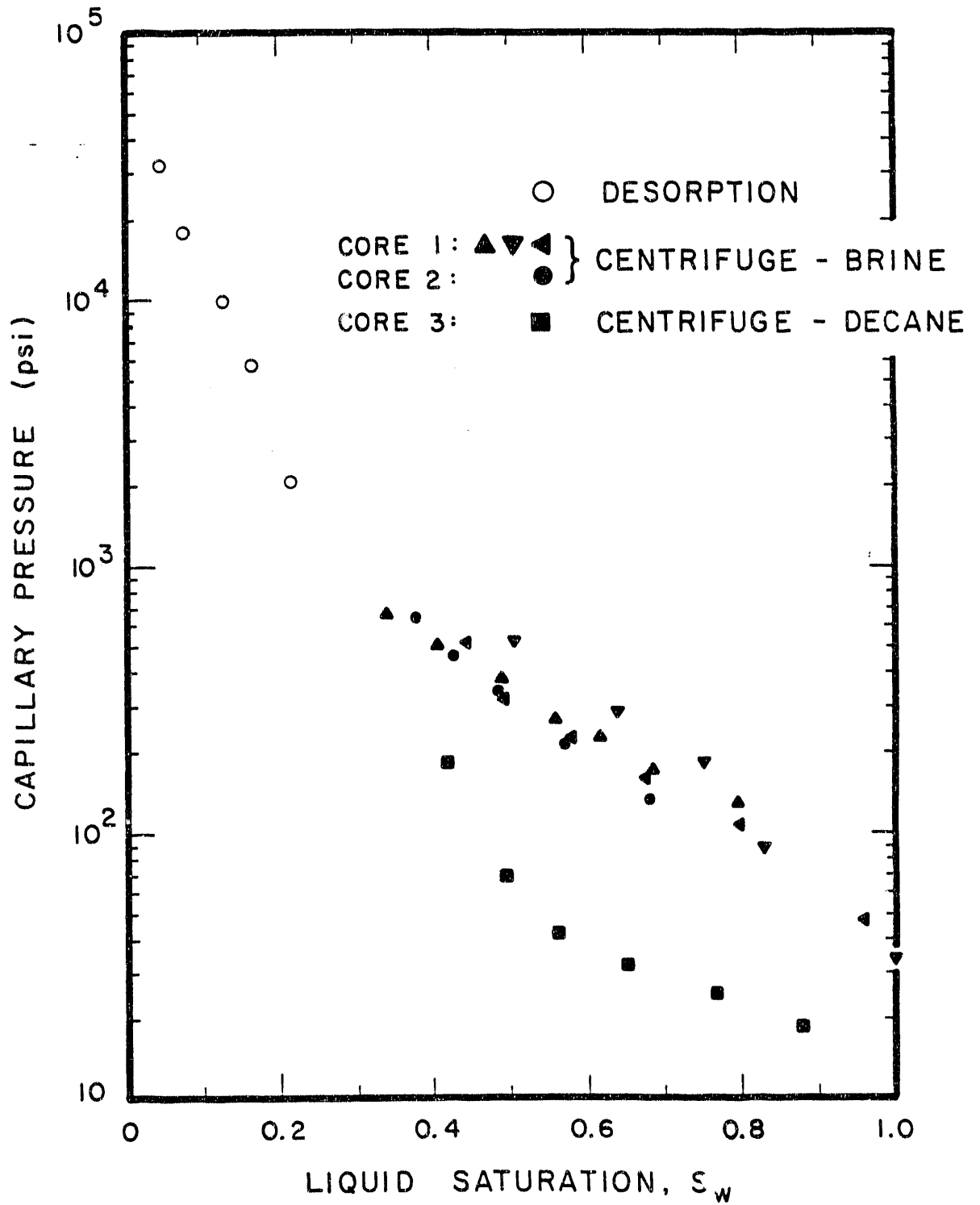


Figure 8

Capillary pressure by combination of centrifuging and desorption: MWX2 51-19.

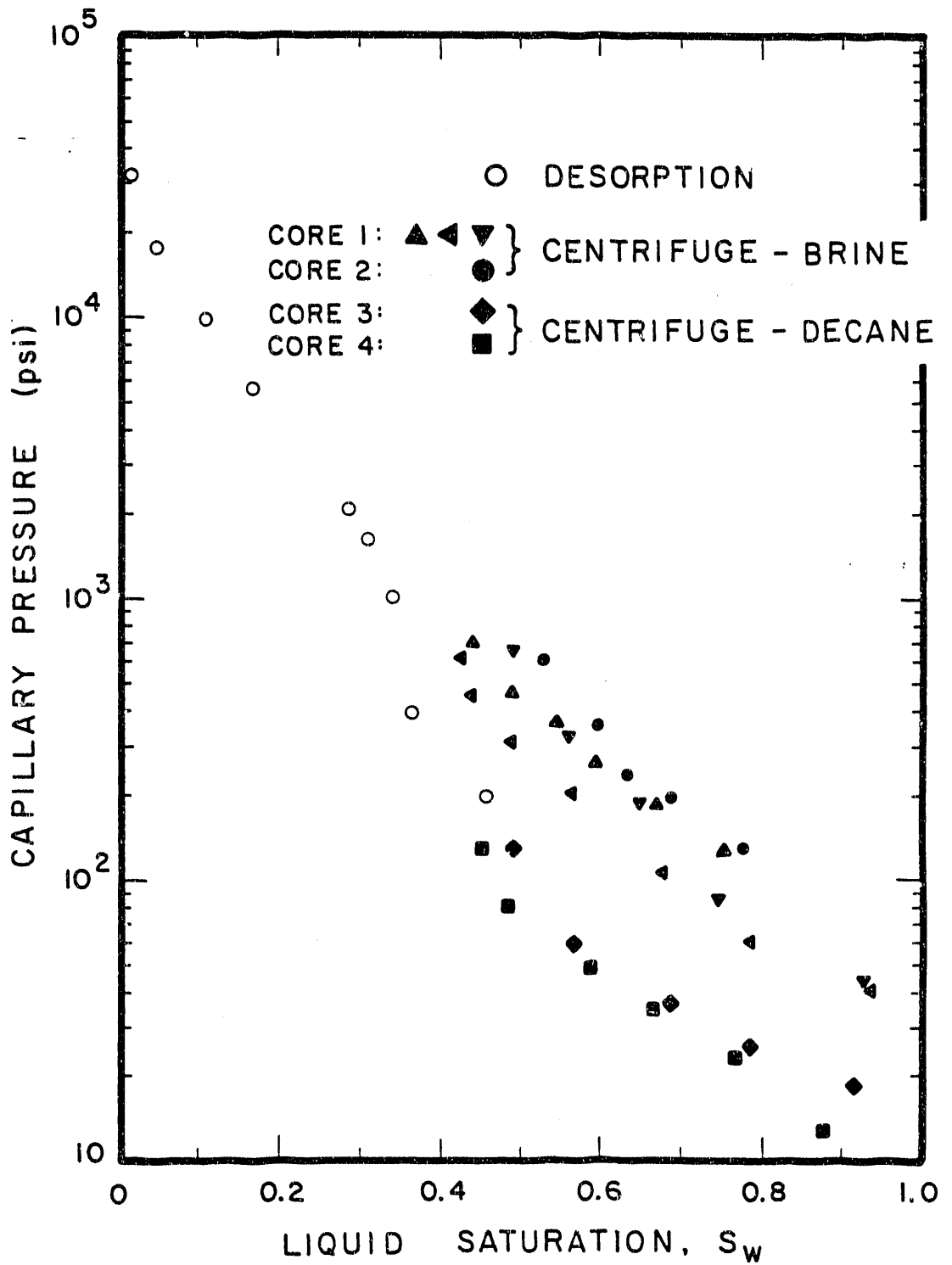


Figure 9

Capillary pressure by combination of centrifuging and desorption: MWX3 64-29.

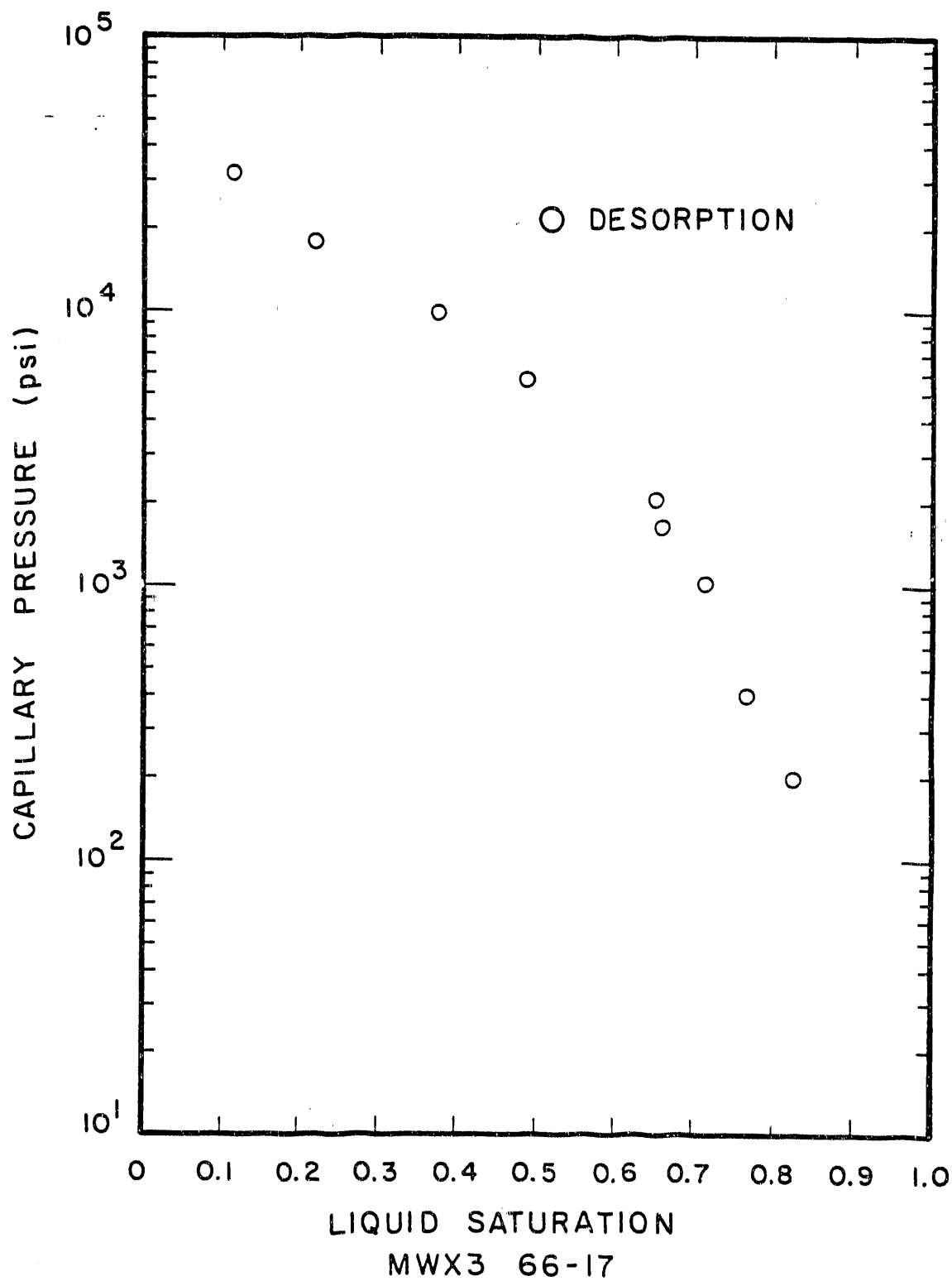


Figure 10 Capillary pressure from desorption experiments.

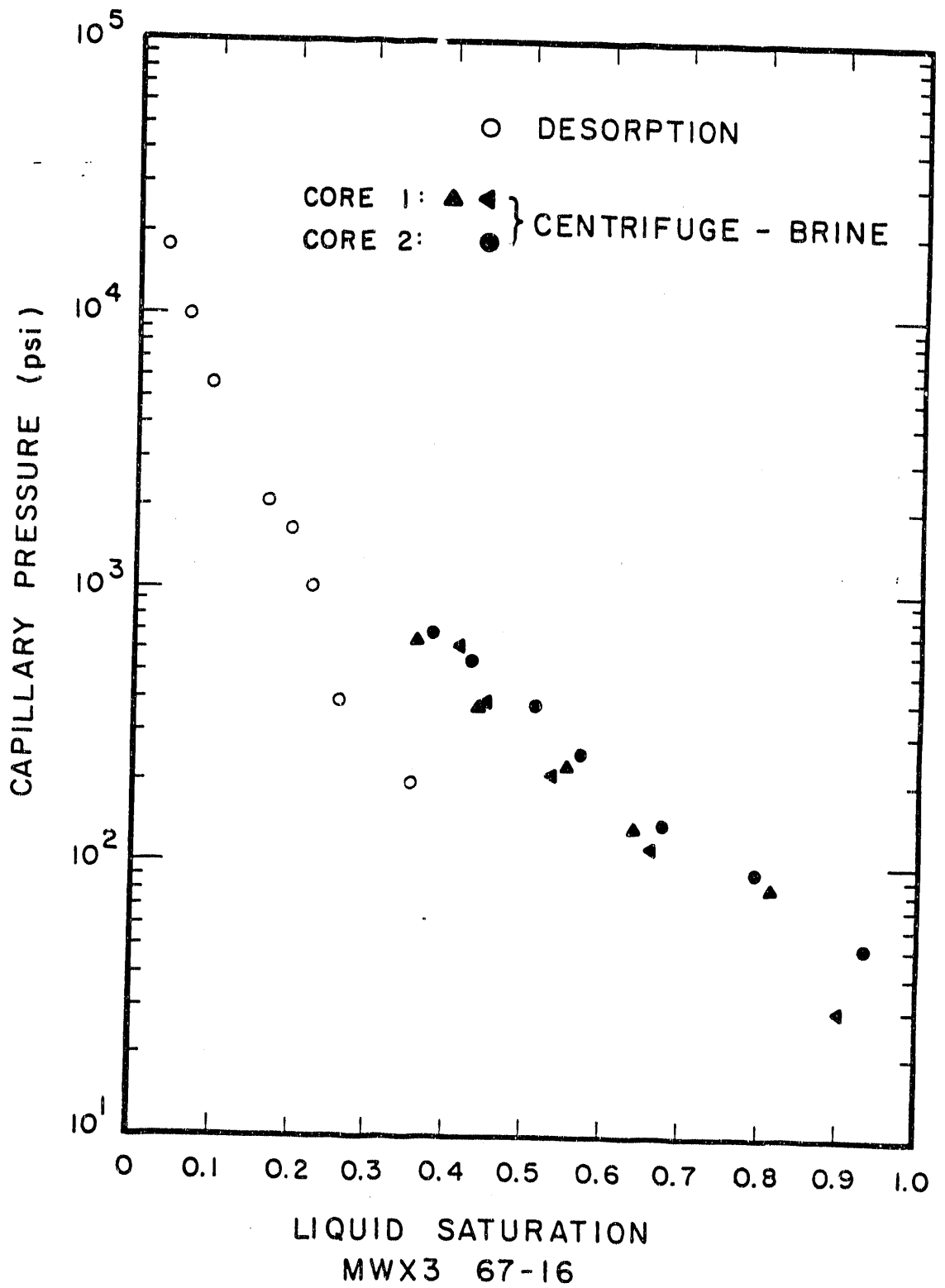


Figure 11 Capillary pressure data from high-speed centrifuge and desorption experiments.

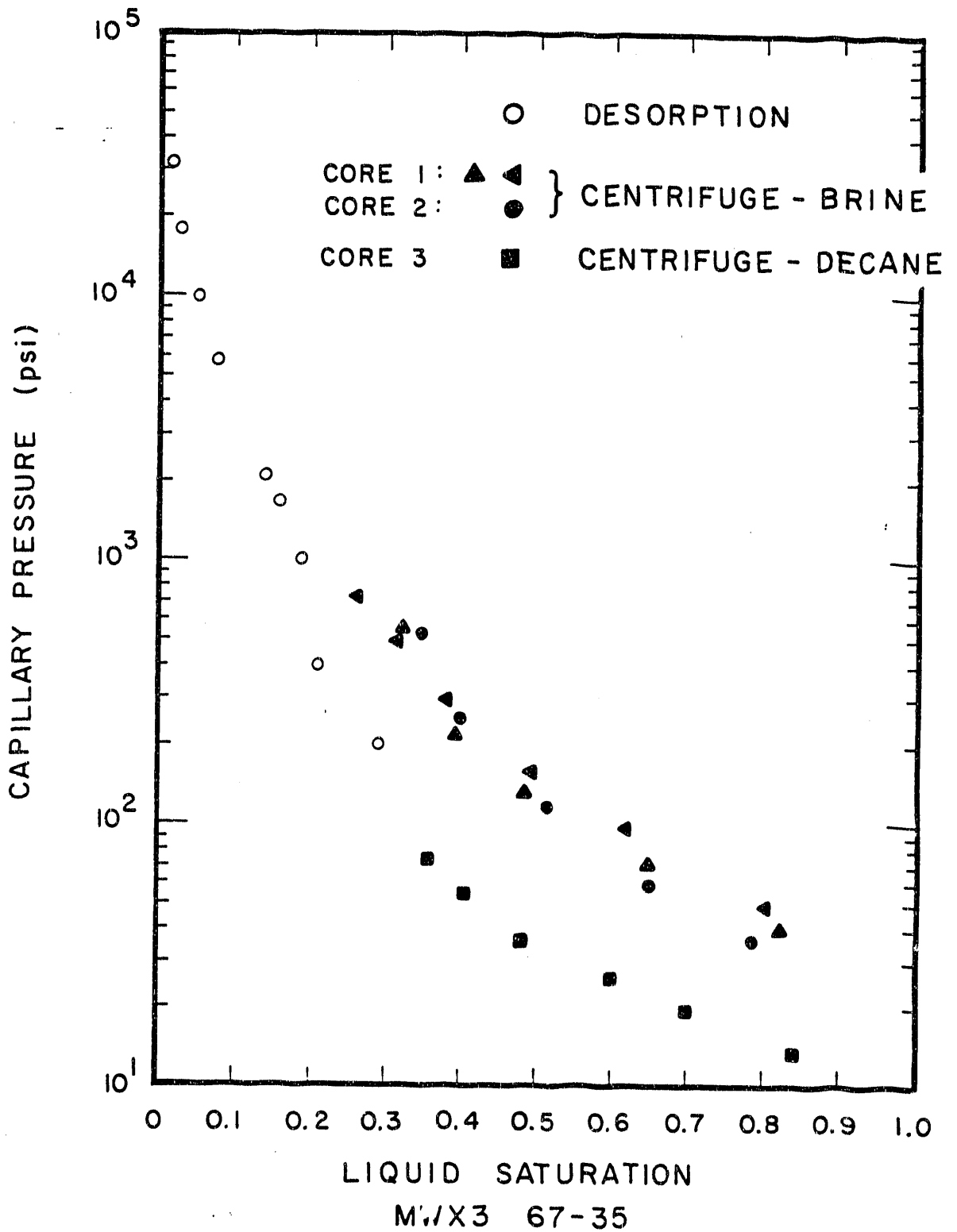


Figure 12 Capillary pressure data from high-speed centrifuge and desorption experiments.

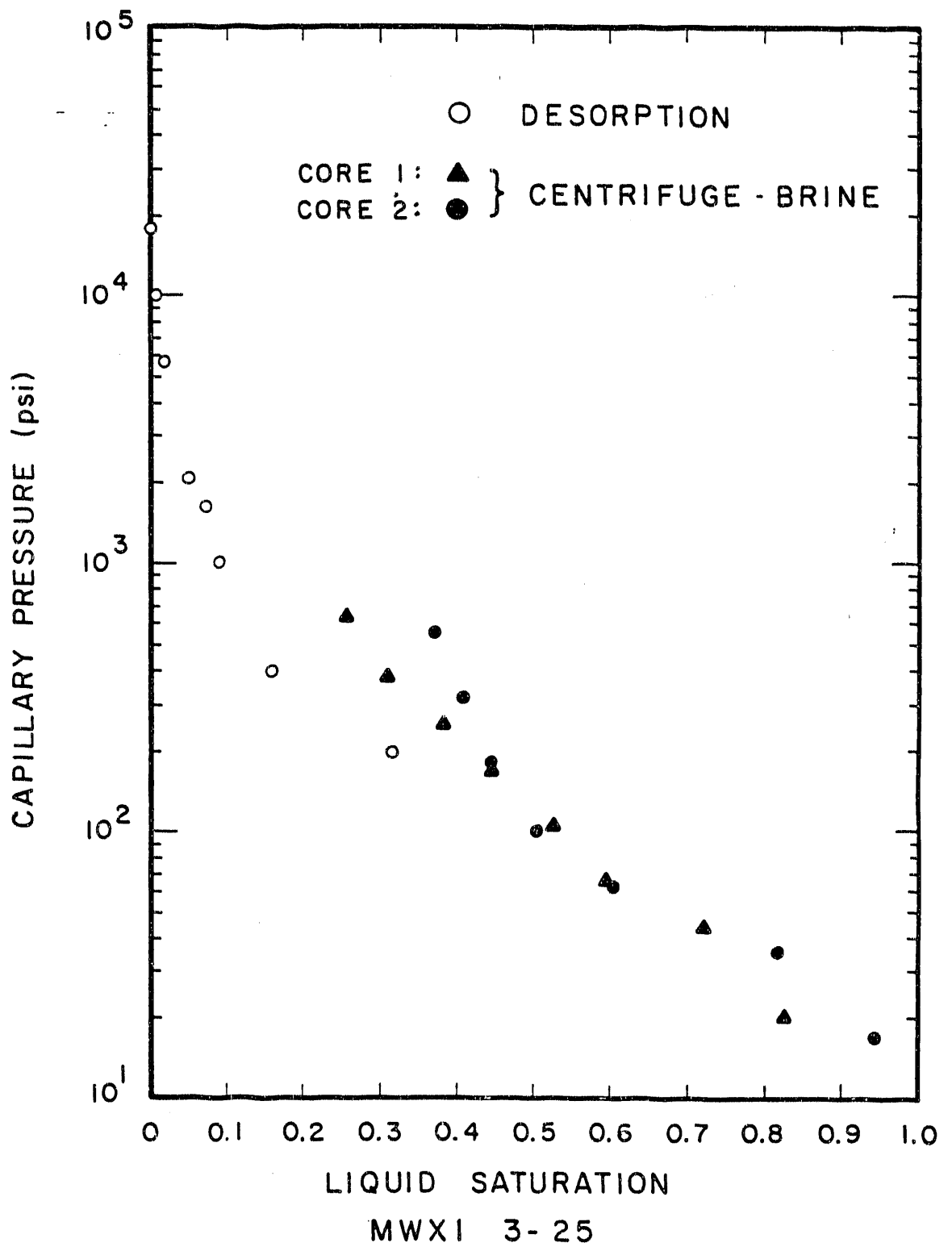


Figure 13 Capillary pressure data from high-speed centrifuge and desorption experiments.

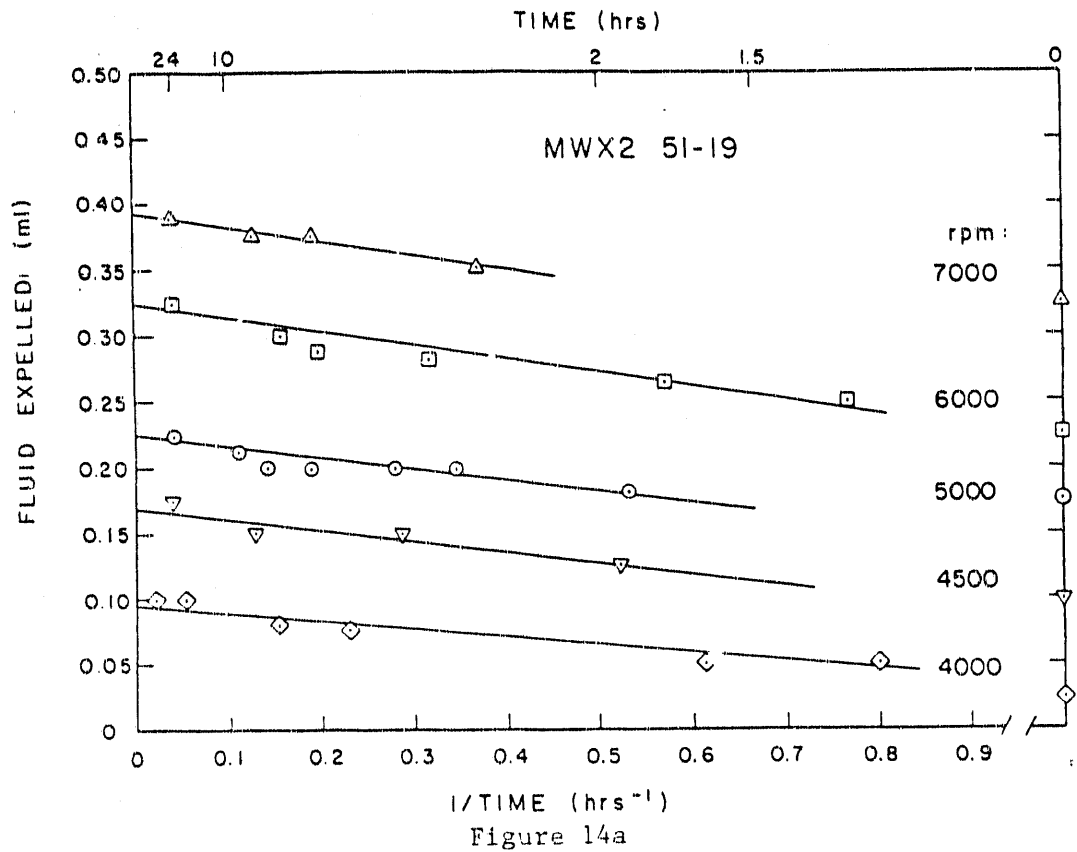


Figure 14a

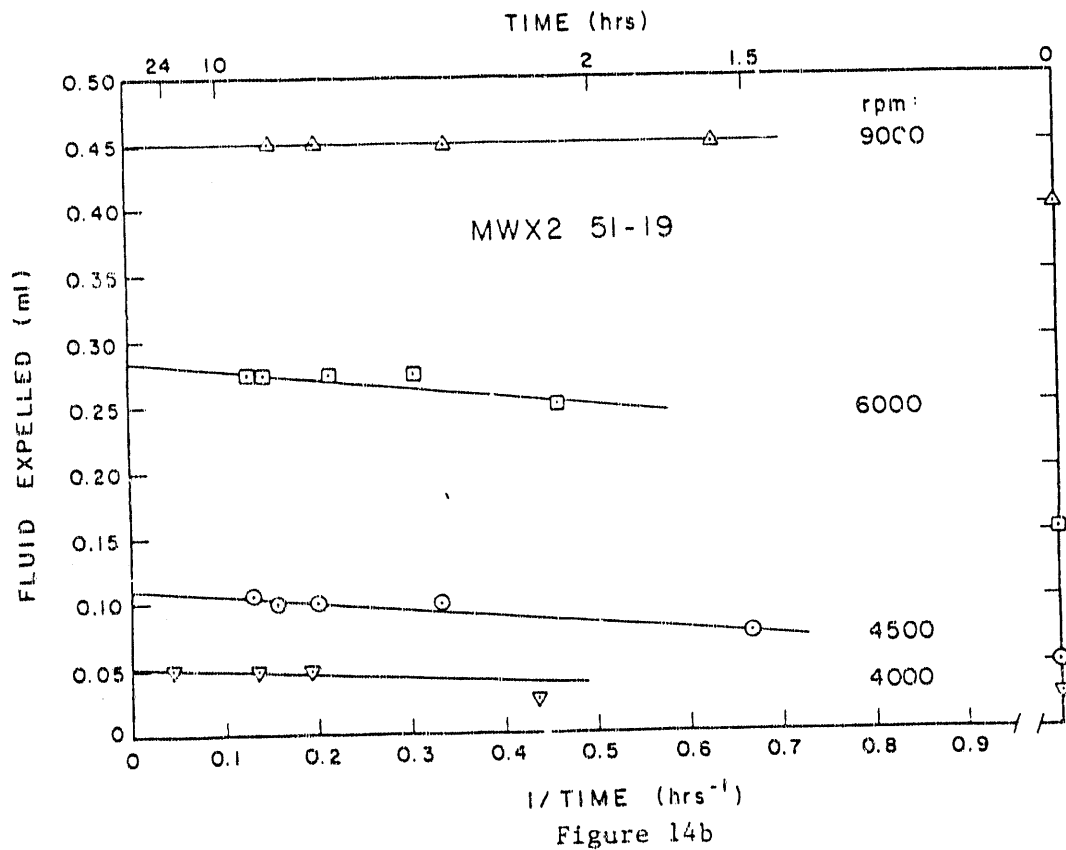


Figure 14b

Equilibration times for air displacing decane at a series of rotational speeds.

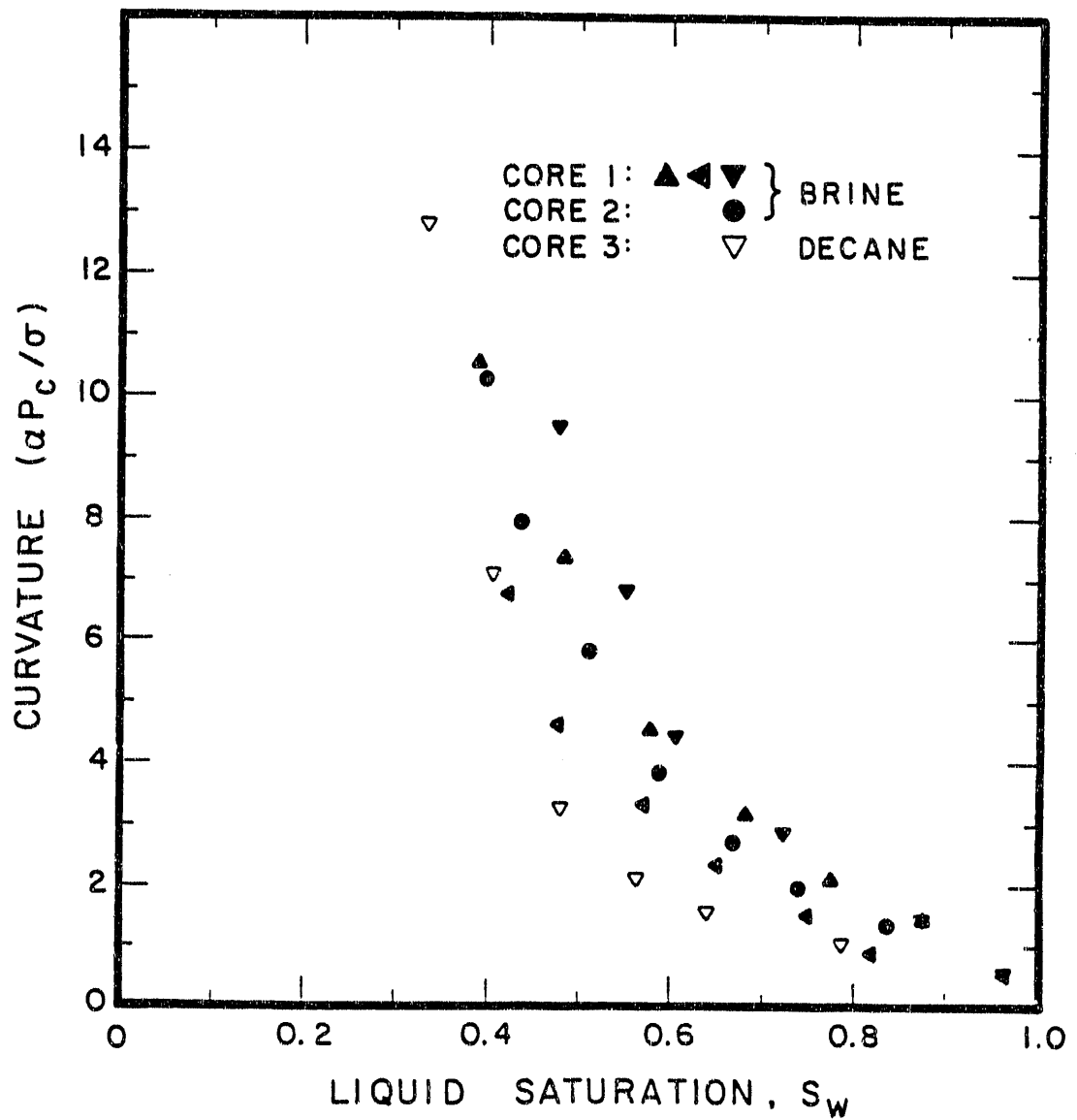


Figure 15

Comparison of displacement curvatures for
brine and decane (both displaced by air)
MWXI 42-25

END

**DATE
FILMED
9/01/92**

